

Experimental and theoretical perspectives on 2-amino 5-bromopyridinium salicylate: a third order nonlinear optical material

D. Prabha¹ · R. Karunathan² · V. Sathyanarayananamoorthi¹

Received: 7 January 2017 / Accepted: 7 March 2017 / Published online: 19 March 2017
© Springer Science+Business Media New York 2017

Abstract Organic charge–transfer complex of 2-amino 5-bromopyridinium salicylate (2A5BPSA) single crystals were grown by slow evaporation solution growth technique using methanol as a solvent. The phases and functional groups of 2A5BPSA have been identified and confirmed through powder X-ray diffraction and Fourier transform infrared. The optical transmittance window and the lower cutoff wavelength of the 2A5BPSA have been identified by UV–Vis–NIR studies. Dielectric studies were carried out for the grown crystals at various temperatures from the frequency ranging from 50 Hz to 5 MHz. Photoconductivity and microhardness studies were also performed for the 2A5BPSA crystal sample. The nonlinear refractive index, nonlinear absorption coefficient have been measured through the Z-scan technique. In addition to that, the quantum chemical calculations on 2A5BPSA have been performed by density functional theory calculations using Hartree–Fock method with HF/6-311++G basis set.

1 Introduction

A fascinating new field of research termed “nonlinear” optics was introduced to the scientific and engineering community after the invention of laser. Nonlinear optics has arisen as one of the most attractive fields of current research in view of its vital applications in areas of optical switching, optical data storage for the developing technologies in telecommunications, frequency mixing, optical parametric oscillation, optical bi-stability, optical logic gates, laser radiation protection, optical image processing, under water communication, biomedical and signal processing analysis optical modulation, second-harmonic generation (SHG), third-harmonic generation (THG) optical signal processing, optical switching, optical data storage devices, frequency shifting, optical modulation, optical switching, optical logic, and optical memory for the emerging technologies in areas such as telecommunications, signal processing and optical interconnections. It is also used in phase conjugation and image reconstruction etc [1–3]. It has been understood that the molecular nonlinearity can be enhanced by large delocalized π -electron systems with strong donor and acceptor groups. The π acceptor charge–transfer (CT) reactions have been employed positively in pharmaceutical investigation. Therefore CT complexes encouraged widespread research on these kinds of complexes [4, 5]. Moreover, the field of non-linear optical materials and electrical conductivities finds the application of such complexes. For these extensive applications, more works on charge-transfer complexes have been carried out. The CT complexes of organic materials are considered for the reason that the special type of interaction is accompanied by transfer of an electron from the donor to the acceptor. Similarly, the protonation of the donor from the acidic acceptors are basis for the construction of ion pair materials. Pyridine and its

✉ V. Sathyanarayananamoorthi
sathyanarayananamoorthi@yahoo.co.in

D. Prabha
dprabha76@rediffmail.com

R. Karunathan
karunathan.phd@gmail.com

¹ PG and Research Department of Physics, PSG College of Arts and Science, Coimbatore 641 014, India

² Department of Physics, Dr. N.G.P. Arts and Science, Coimbatore 641 048, India

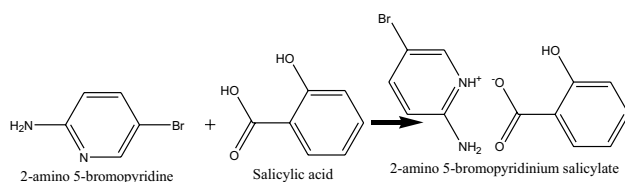
organic complexes exhibit a large amount of fluorescence in crystal environment and also these compounds has many biological, chemical, nonlinear optical and medical applications and has the tendency to form the stable compounds [6]. Also pyridine-acid based derivatives are promising NLO materials due to its conjugated donor- π -acceptor bond which give raise to a strong π -electron delocalization and its strong hydrogen bonding [5–7]. Several pyridinium-acid based SHG and THG compounds were synthesized and their properties are extensively studied [8–12].

2-Amino 5-bromopyridine is one of such compound which easily forms hydrogen bonding between the suitable acids. Salicylic acid is a carboxylic acid well-known for its optical and biological applications. Previously effect of solvents on the growth and solvent less growth were reported [13, 14]. 2-Amino 5-bromopyridinium salicylate is a donor-acceptor based organic CT complex which structure was previously reported by Ching Kheng Quah [15]. Based on this in the present work we report the crystal growth and characterization studies including powder XRD, Fourier transformation infra-red (FTIR), UV-Vis studies, dielectric, photoconductivity, microhardness, TG/DTA and Z-scan, studies of 2A5BPSPA. Also density functional theory (DFT) calculations with HF/6-311++ basis set have been carried to study the, molecular electrostatic potential, HOMO-LUMO and natural bonding analysis of 2A5BPSPA. The studies here are reported for the first time in literature, to the best of our knowledge.

2 Experimental details

2.1 Material synthesis

The pure specimens of 2-amino 5-bromopyridine and salicylic acid were used without further purification for material synthesis. The two reactants were dissolved separately with 1:1 molar ratio in methanol and mixed together. The resulting solution was stirred well for about 1 h. The obtained microcrystalline product was filtered off and then purified by repeated recrystallization process in methanol. The recrystallized compound was used for single crystal growth by the solvent evaporation technique. The reaction of 2A5BPSPA was shown Scheme 1.



Scheme 1 Reaction scheme of 2A5BPSPA with methanol as a solvent

2.2 Crystal growth

It is easy to grow single crystals of optical quality of 2A5BPSPA using a standard slow evaporation technique. A saturated solution of 2A5BPSPA in methanol was prepared and stirred well about one and half hour to dissolve the material completely. The solution was then filtered through a quantitative whatmann 41 grade filter paper to remove the suspended impurities. The beaker containing the filtrate was covered using thin polythene sheet to prevent the evaporation quickly. The perforations were made to regulate the evaporation. The beaker was kept aside unperturbed in an atmosphere most suitable for the growth of single crystals. Proper care was taken to minimize mechanical disturbance and temperature fluctuations. In a normal growth period of 12 days, single crystals of the title material were harvested and subjected to the characterization. The photograph of the grown crystal is shown in Fig. 1.

3 Results and discussion

3.1 X-ray diffraction analysis

The obtained unit cell parameters are $a=8.92 \text{ \AA}$, $b=10.87 \text{ \AA}$ $c=13.18 \text{ \AA}$ and $\beta^\circ = 108.71$. From the single crystal XRD it is concluded that grown crystal belongs to monoclinic system with the space group of $P2_1/c$. The

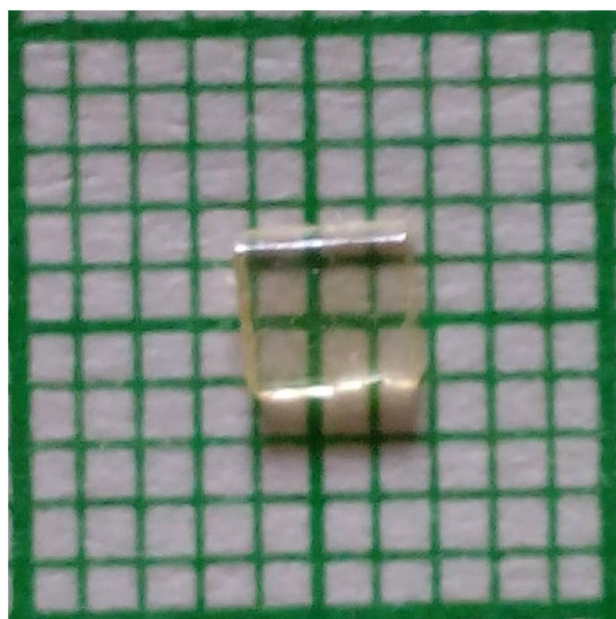


Fig. 1 As grown crystal of 2A5BPSPA

obtained lattice parameter values are in good agreement with the earlier reported values [15]. Powder X-ray diffraction pattern for the grown crystals were carried out by using RICH SEIFERT diffractometer. Diffraction pattern data were collected on the diffractometer equipped with monochromatic $\text{CuK}\alpha$ radiation (1.540598 Å) and detected by a scintillation counter. The sample was scanned for 2θ values from the range 10° – 50° at the scan rate of 1° per minute. The obtained diffraction pattern was compared with the theoretical simulated XRD pattern which is generated from crystallographic information file (.cif) using mercury software shown in Fig. 2. The sharp and well defined Bragg's peaks confirm the crystallinity of the grown sample.

3.2 FTIR analysis

The functional groups of 2A5BPSA were identified by FTIR spectrum in the range 4000 – 400 cm^{-1} as shown in Fig. 3. A peak at 3339 and 3072 cm^{-1} is due to the stretching vibrations of N-H and NH_3^+ . The OH stretching vibration of salicylic acid was found at 3338 cm^{-1} . The C=O vibration of COO- in salicylate gives band at 1688 cm^{-1} . The absorptions at 804 and 758 cm^{-1} is assigned to the C-C and C-H out of plane bending vibrations whereas a band at 1248 cm^{-1} is ascribed to the C-H in-plane bending vibration. The C-O stretching and C-C out of plane bending vibration absorb frequency at 1248 and 668 cm^{-1} respectively. The presence of C-C skeletal vibration is confirmed due to the presence of peaks at 1079 and 957 cm^{-1} . The aromatic C-H stretching vibration was observed at 2730 cm^{-1} . The aromatic C=O and C=N stretching vibrations occurred at 1688 and 1586 cm^{-1} respectively. A peak at 1455 cm^{-1} is assigned to N-H bending vibration. The in-plane and out of plane bending vibrations was observed at

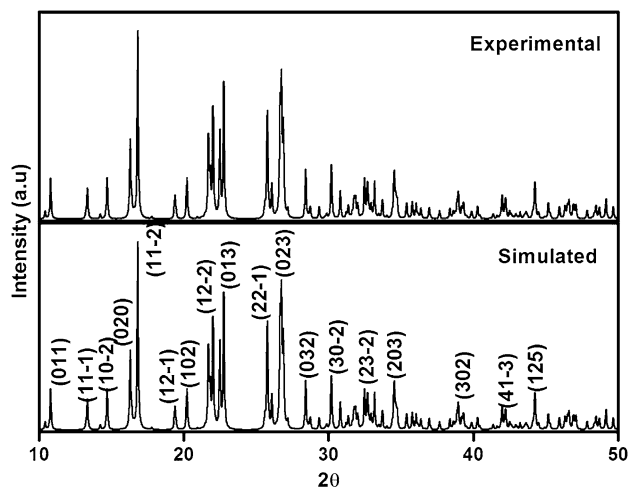


Fig. 2 Powder XRD pattern of 2A5BPSA

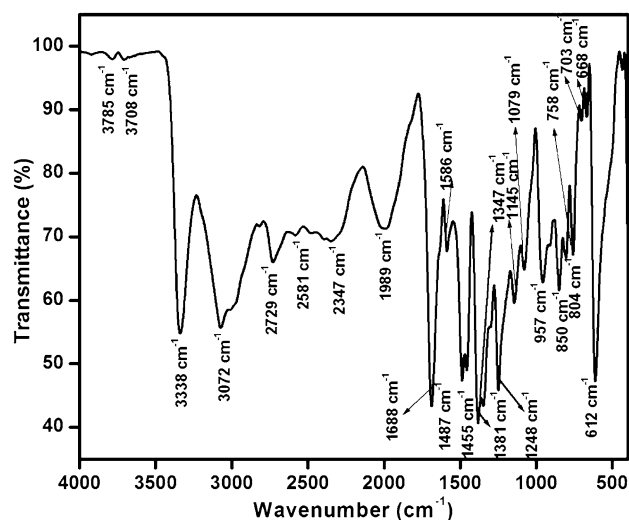


Fig. 3 FTIR spectrum of 2A5BPSA

850 cm^{-1} . The stretching vibrations of C-Br occurred at 613 cm^{-1} . Thus, the existence of functional groups of title compound was identified.

3.3 UV-Vis-NIR spectral analysis

The grown crystals of 2A5BPSA with thickness about 2 mm were subjected to UV-Vis-NIR spectral analysis in the wavelength range from 200 to 1200 nm, with the help of Varian Cary UV-Vis-NIR spectrophotometer. The UV-Vis-NIR spectral analysis is one of the important analyses to study linear optical characteristics of the crystal. Ultra violet and visible radiation causes the electron transitions from the ground to a high energy state in the material. UV absorption spectra arise from the transition of electrons within a molecule from a lower electronic energy state to higher energy state. When an atom or molecule absorbs the energy, electrons are promoted from their ground state to an excited state. The comparison of absorbance spectrum of the title compound with the parent compound is depicted in the Fig. 4a. For pure pyridine two absorption peaks were observed at 237 and 318 nm whereas salicylic acid exhibits the bands at 210 and 296 nm. For the title compound the spectrum reveals that the strong absorption band appears around 244 nm is attributed to the $n-\pi^*$ transition. The variation in the absorption spectrum confirms the CT of the compound. The improved optical transmittance is one of the most important properties in the NLO crystalline compounds. The transmittance spectrum is depicted in the Fig. 4b. From the spectrum, it is clear that UV cut-off wavelength of grown crystal is noted around 244 nm. The crystal is entirely transparent beyond cut-off wavelength up to 1200 nm. The transparent character of crystal is suitable

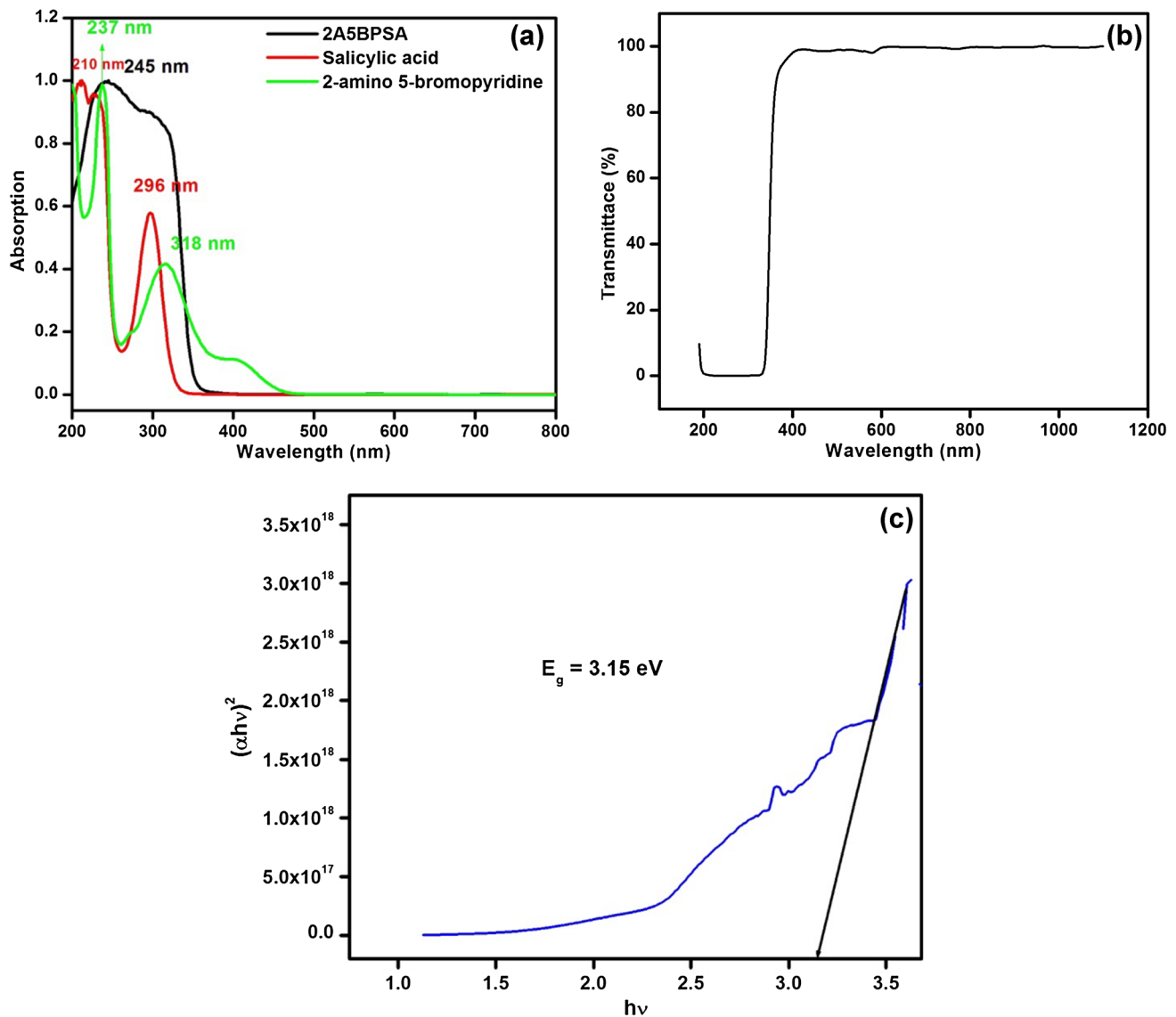


Fig. 4 **a** Optical absorption spectrum of 2A5BPSA, **b** optical transmittance spectrum of 2A5BPSA, **c** optical band gap of 2A5BPSA

and prerequisite for THG of wavelength [16–18]. The optical absorption coefficient (α) was calculated from the transmittance using the given formula

$$\alpha = \frac{2.3036 \log (1/T)}{d} \quad (1)$$

where T is the measured crystal transmittance and d is the thickness of the sample. Assuming parabolic trends, the relation between α and E_g is given by

$$\alpha = \frac{A(h\nu - E_g)^n}{h\nu} \quad (2)$$

where A is a constant, E_g is the optical band gap of the material, ν is the frequency of the incident photon and

h is the planks constant. Fig 4a shows the plot of $h\nu$ and $(\alpha h\nu)^2$. According to the Tauc plot the optical band gap of the material was obtained by extrapolating the linear portion of the plots of $(\alpha h\nu)^2$ and $h\nu$ [19, 20]. The optical band gap was found to be 3.15 eV. Crystals with wide band gap expected to possess high laser damage threshold and large transmittance in the visible region [21].

3.4 Dielectric analysis

The dielectric constant is one of the basic electrical properties of solids. The dielectric properties were measured of the crystal using HIOKI 3532-50 LCR Hi-TESTER. The frequency dependent dielectric constant (ϵ_r) and

dielectric loss ($\tan \delta$) of the crystal were measured at a temperature range of 303–363 K, in the frequency range of 50Hz–5 MHz. The sample was polished smoothly, covered by the silver paste, and the mounted between two electrodes and thus a parallel plate capacitor was formed. The relative dielectric constant and dielectric loss were measured grown 2A5BPSA single crystal as a function of frequency as shown in Fig. 5a, b. The figure shows the variation of the dielectric constant and dielectric loss, respectively at different frequencies measured at different temperature. From the curve, the dielectric constant and dielectric loss decrease with increasing frequency because the different polarization mechanisms cannot withstand at high frequencies [22]. The low values of dielectric constant at higher frequencies are important for these materials in the construction of photonic, microelectronic, NLO devices and also low dielectric loss indicates that the grown crystal contains very low density of defects [23].

3.5 Photoconductivity

Photoconductivity of the grown 2A5BPSA crystal was studied using a Keithley 6517B electrometer. The experiment was performed at room temperature and the applied electric field was increased from 10 to 100 V/cm, and corresponding dark current was recorded. For the same set of applied voltage, the sample was then exposed to the radiation from 100 W halogen lamp and the photo current was measured. Figure 6 shows the plot of dark current and photo current against electric field. It is observed that both the dark and photo currents increase linearly with the applied electric field. But the photo current is more compared to the dark current which is termed as positive

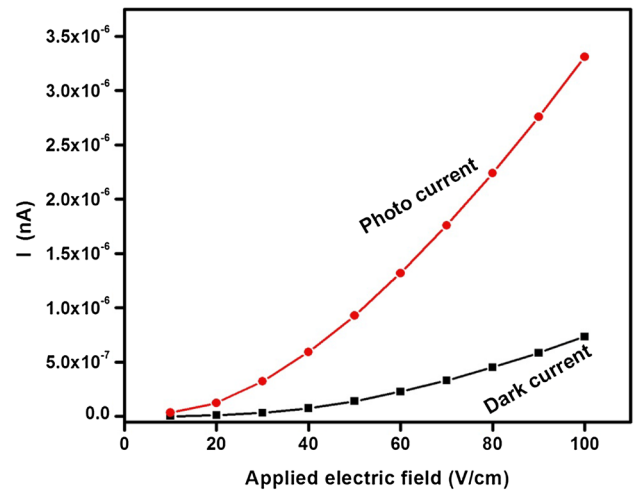


Fig. 6 Variation of dark and photo current with applied field

photoconductivity. The grown 2A5BPSA crystal exhibits the positive photoconductivity in nature. This may be due to the generation of mobile charge carriers caused by the absorption of photon [24].

3.6 Microhardness studies

Microhardness study is a measure of resistance it offers to local deformation. Also it provides useful information such as hardness number, strength and yield stress and which is strongly related to the molecular structure and material composition [25, 26]. Microhardness indentation was made on crack free and optically clear surface of the grown crystal for different loads ranging from 10 to 100 g with a

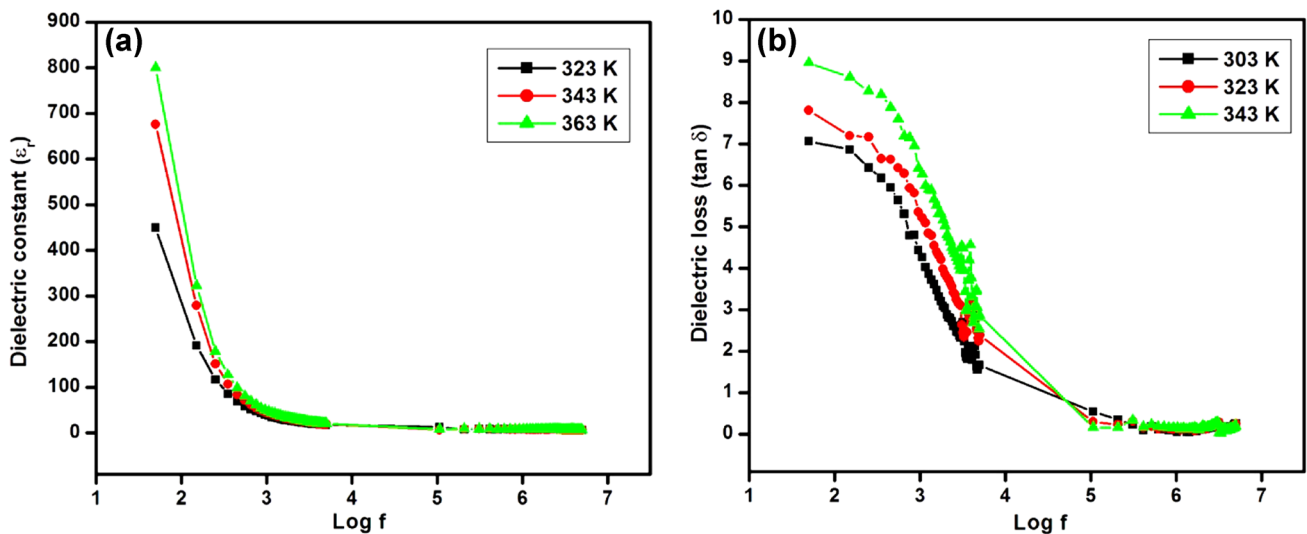


Fig. 5 a Dielectric constant versus log f, b dielectric loss versus log f

constant indentation time of 10 s at room temperature. The vicker's hardness number H_v of the crystal was calculated from the standard formula

$$H_v = 1.8544 (P/d^2) \text{ kg mm}^{-2} \quad (3)$$

where H_v is the Vicker hardness number in kg/mm^2 , P is the applied load in kg, and d is the mean diagonal length of the indenter impression in millimeter. Figure 7a shows the variation of H_v as a function of the applied field. It is very clear from the figure that the hardness value increases with increase in load and the crystal exhibits the reverse indentation size effect (RISE). On further increase in the load above 100 g micro cracks were observed, owing to the release of internal stress generated locally by a deformation. The plot of $\text{Log } P$ against $\text{Log } d$ gives the value of n and it is determined to be 2.65 (Fig. 7b). According to Onitsch and Hanneman n should lie between 1 and 1.6 for harder materials and above 1.6 for softer materials [27, 28]. Hence the grown LPBN crystal belongs to the soft material category.

3.7 TG/DTA analysis

Thermo gravimetric (TG) and differential thermal analysis (DTA) gives useful information regarding phase transition and different stages of decomposition of the compound. To study the thermal stability of the grown crystal TG/DTA analysis were carried out using SDT Q 600 V 8.3 instrument from room temperature to 500°C in nitrogen atmosphere at a heating rate of $20^\circ\text{C}/\text{min}$. Figure 8 shows the TG/DTA analysis for the grown crystals. From the TG curve it is observed that the crystal undergoes two stage decompositions occurred between $130\text{--}150^\circ\text{C}$ and $150\text{--}214^\circ\text{C}$. The first stage of decomposition is due to the liberation of volatile substance

like, CO , CO_2 , CH_4 and NH_3 molecules. The second stage is attributed to the melting of the compound. In DTA there is a sharp endothermic at 214°C is assigned to melting point of the compound which are fit well with the TG spectrum. TG/DTA curve indicate that there are no endothermic or exothermic transitions below the 100°C . This shows that the absence of water molecules in the crystalline lattice.

3.8 Z-scan studies

The Z-scan study of the 2A5BPSA crystals was studied by the Z-scan technique. Generally this technique is used to determine the both nonlinear absorption coefficient (β) and nonlinear refraction (n_2). It is based on a spatial distortion and offers simplicity as well as high sensitivity [29, 30]. To study the nonlinear refraction by this method depends on the position of the sample under investigation along a focused Gaussian laser beam. He–Ne laser with a fundamental wavelength of 632.8 nm with a repetition rate of 1 kHz was used. In the present investigation, the sample translated in the Z-direction along the axis of a focused Gaussian beam and the far field intensity was measured as a function of the sample position. Figure 9a, b shows the normalized transmittance T with the open and closed aperture as a function of distance Z along the lens axis in the far field. The measurable quantity ΔT_{p-v} , the difference between the peak and valley transmittances, $T_p - T_v$ as a function of $|\Delta\Phi|$ is given by

$$\Delta T_{p-v} = 0.406 (1 - S)^{0.25} |\Delta\Phi| \quad (4)$$

where s is the linear aperture transmittance and $|\Delta\Phi|$ is the on-axis phase shift.

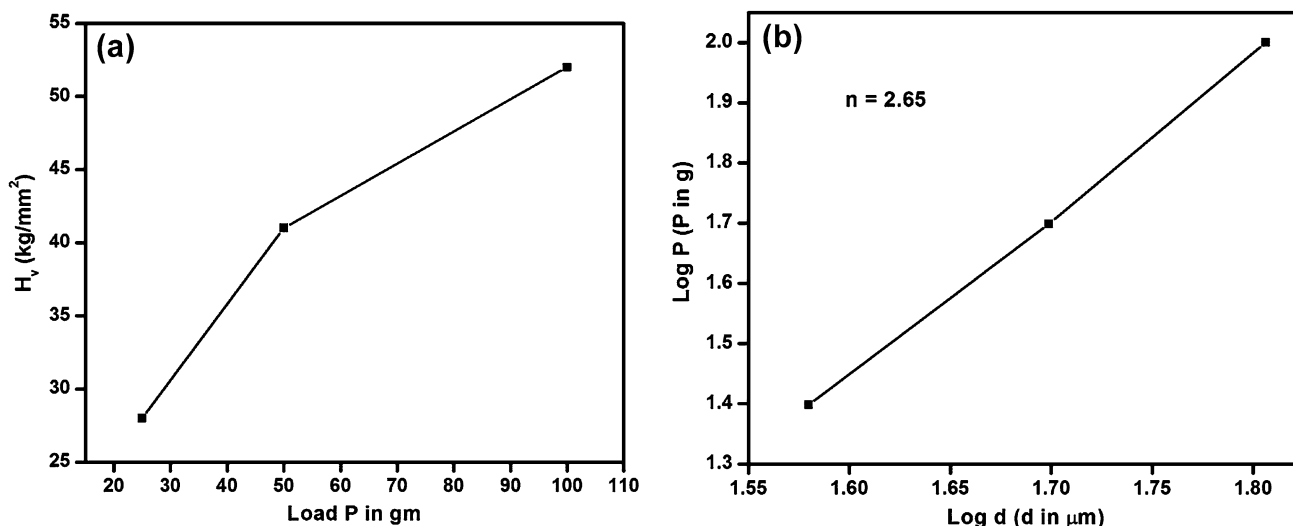


Fig. 7 a Vicker's hardness number with load, b $\text{Log } P$ versus $\text{Log } d$

Fig. 8 TG/DTA spectrum of 2A5BPSA

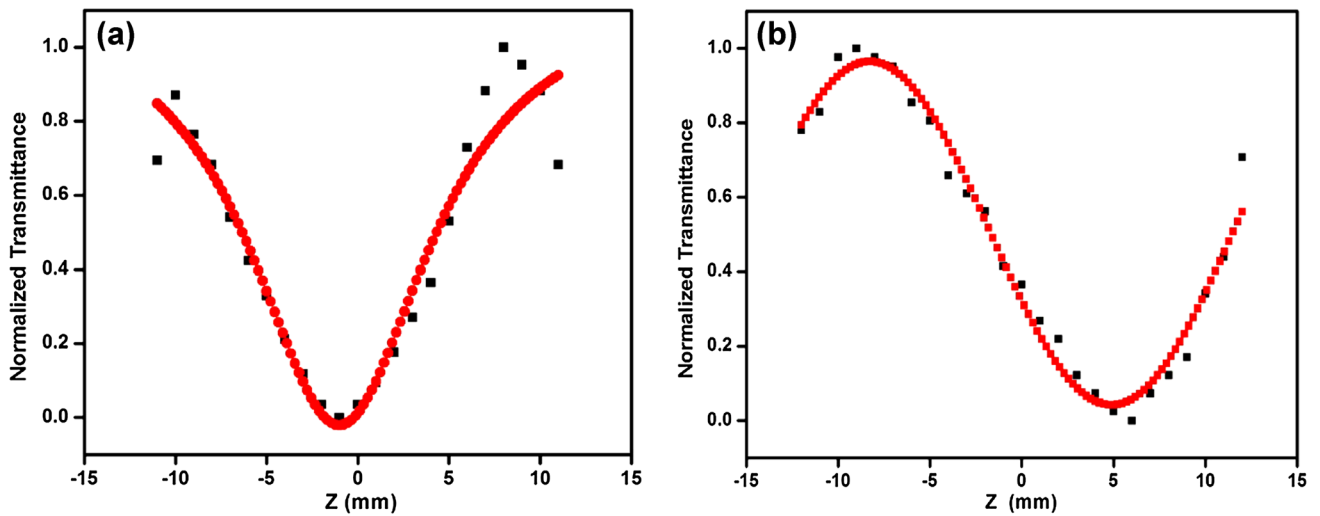
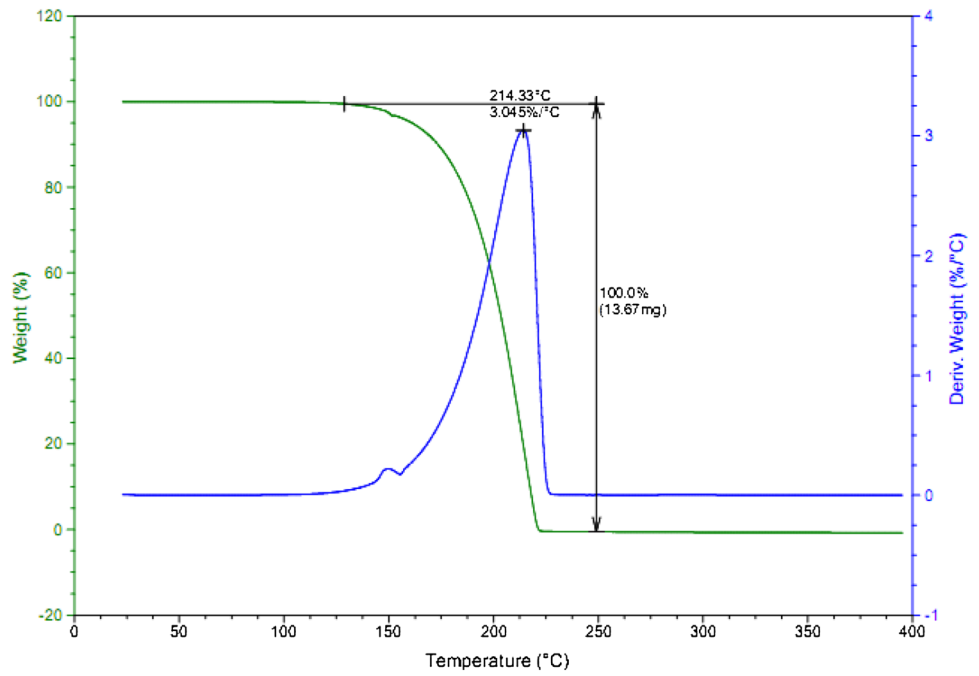


Fig. 9 **a** Normalized transmittance with open aperture as a function of Z position. **b** Normalized transmittance with closed aperture as a function of Z position

$$S = 1 - \exp\left(\frac{-2r_a^2}{\omega_a^2}\right) \tag{5}$$

where r_a is the radius of aperture and ω_a is the beam radius at the aperture. The on-axis phase shift is related to the third order nonlinear refractive index.

$$n_2 = \frac{\Delta\Phi}{kI_0L_{eff}} \tag{6}$$

$$L_{eff} = \frac{1 - e^{-\alpha L}}{\alpha} \tag{7}$$

$$\beta = \frac{2\sqrt{2} \Delta T}{I_0 L_{eff}} \tag{8}$$

The real and imaginary parts of the third order nonlinear optical susceptibility were determined from the experimental determination of n_2 and β according to the following relations:

$$\operatorname{Re}\chi^{(3)}(\text{esu}) = 10^{-4} \frac{(\epsilon_o C^2 n_o^2 n^2)}{\pi} \left(\frac{\text{cm}}{\text{W}} \right) \quad (9)$$

$$\operatorname{Im}\chi^{(3)}(\text{esu}) = 10^{-2} \frac{(\epsilon_o C^2 n_o^2 \lambda \beta)}{4\pi^2} \left(\frac{\text{cm}}{\text{W}} \right) \quad (10)$$

The absolute value of $\chi^{(3)}$ was calculated from the following relation.

$$|\chi^{(3)}| = [(\operatorname{Re}\chi^{(3)})^2 + (\operatorname{Im}\chi^{(3)})^2]^{\frac{1}{2}} \quad (11)$$

The nonlinear refractive index (n_2) and nonlinear absorption coefficient (β) are calculated from the normalized transmittance curve. The estimated nonlinear refractive index, nonlinear absorption coefficient and third order susceptibility values of 2A5BPSA are $4.67302 \times 10^{-8} \text{ cm}^2/\text{W}$, $1.786 \times 10^{-4} \text{ cm/W}$ and $1.08076 \times 10^{-7} \text{ esu}$ (Table 1). The obtained positive refractive index was mainly due to the thermo-optic effect on the crystal samples [31].

3.9 Molecular electrostatic potential

A molecule of electrostatic potential map provides information about the electron acceptor and electron-donor regions. Using this information, we can estimate intramolecular and intermolecular hydrogen bonds may present between the atoms. The different values of the electrostatic potential at the surface are represented by different colors; red represents regions of most electro negative electrostatic potential, blue represents regions of most positive electrostatic potential and green represents regions of zero potential (Fig. 10a–d). The molecular electrostatic potential maps were calculated. The colour scheme for the MEP surface is red, electron rich, partially negative charge; blue, electron deficient, partially positive charge; light blue,

slightly electron deficient region; yellow, slightly electron rich region; green, neutral; respectively. The figure indicates that the region around the oxygen atom represents the most negative potential region (red). The predominance of light green region in the MEP surfaces corresponds to a potential half-way between the two extremes red and dark blue colour. The value of electrostatic potential is tends to $-7.268 \times 10^{-2} - 7.268 \times 10^{-2}$. The maximum and minimum values for the total electron density are -1.766×10^{-2} to 1.766×10^{-2} , respectively. In here, the red regions settled in O_2 atom. So, O_2 atom can be estimated to be electron-donors. The blue colour occupied on the almost whole molecule. This estimate was confirmed by the C17–O18...H13 and C1–N8...NH₂ hydrogen-bonding in the crystal structure.

3.10 Frontier molecular orbital (FBO) analysis

The theoretical quantum chemical studies were performed at Hartee–Fock method with HF/6-311++G basis set using Gaussian 09 programme [32–38]. GaussView 5.0 visualization program [37] has been employed to shape HOMO, LUMO orbitals.

Highest occupied molecular orbital (HOMO) and lowest lying unoccupied molecular orbital (LUMO) are called as frontier molecular orbitals (FMOs). The FMO plays a major role in the optical and electrical properties as well as in the quantum chemistry. The HOMO (outermost orbital) represents the ability to act as an electron donor and directly related to the ionization potential whereas the LUMO acts as an electron acceptor and directly related to the electron affinity. The highest and second highest occupied MO's (HOMO and HOMO –1), the lowest and the second lowest unoccupied MO's (LUMO and LUMO+1) were also calculated.

The atoms occupied by more densities of HOMO should have stronger ability for detaching electrons, whereas the atom with more occupation of LUMO should be easier to gain electron. For 2-amino 5-bromopyridinium salicylate, the highest occupied molecular orbital (HOMO) lying at -4.9043 eV , is a delocalized π orbital. The HOMO –1, lying -8.9142 eV below the HOMO, is a delocalized π orbital over both the entire molecules. Although, the HOMO –2, lying -9.3643 eV below the HOMO, respectively, are π orbitals that localized in aromatic ring. Whereas, the lowest unoccupied molecular orbital (LUMO), lying at 0.5798 eV , is π^* orbital that localized for the total molecule. The LUMO+1 and LUMO+2 lying about 1.0054 and 1.2778 eV above the LUMO it is also a π^* that is similar to LUMO. The positive phase is red and the negative one is green in the figure. It is clear from the figure that, while the HOMO is localized on approximately the whole molecule, LUMO is localized on the

Table 1 Evaluated third-order nonlinear properties of 2A5BPSA crystal

Laser beam wave length (λ) = 632.8 nm
Laser power (P) = 35 mW
Beam radius of the aperture (ω_a) = 1 mm
Beam radius (ω_o) = 12.22 μm
Incident intensity at the focus ($Z=0$) = 1 MW/cm ²
Lens focal Length (f) = 24 cm
Optical path distance (Z) = 175 cm
Effective thickness (L_{eff}) = 3 mm
Aperture radius of detector for closed (r_a) = 4 mm
Aperture radius of detector for open (r_a) = 30 mm
Incident intensity at the focus ($Z=0$) = 2 mW/cm ²
Nonlinear refractive index (n_2) = $4.67302 \times 10^{-8} \text{ cm}^2/\text{W}$
Nonlinear absorption coefficient (β) = $1.786 \times 10^{-4} \text{ cm/W}$
The third-order nonlinear susceptibility ($\chi^{(3)}$) = $1.08076 \times 10^{-7} \text{ esu}$

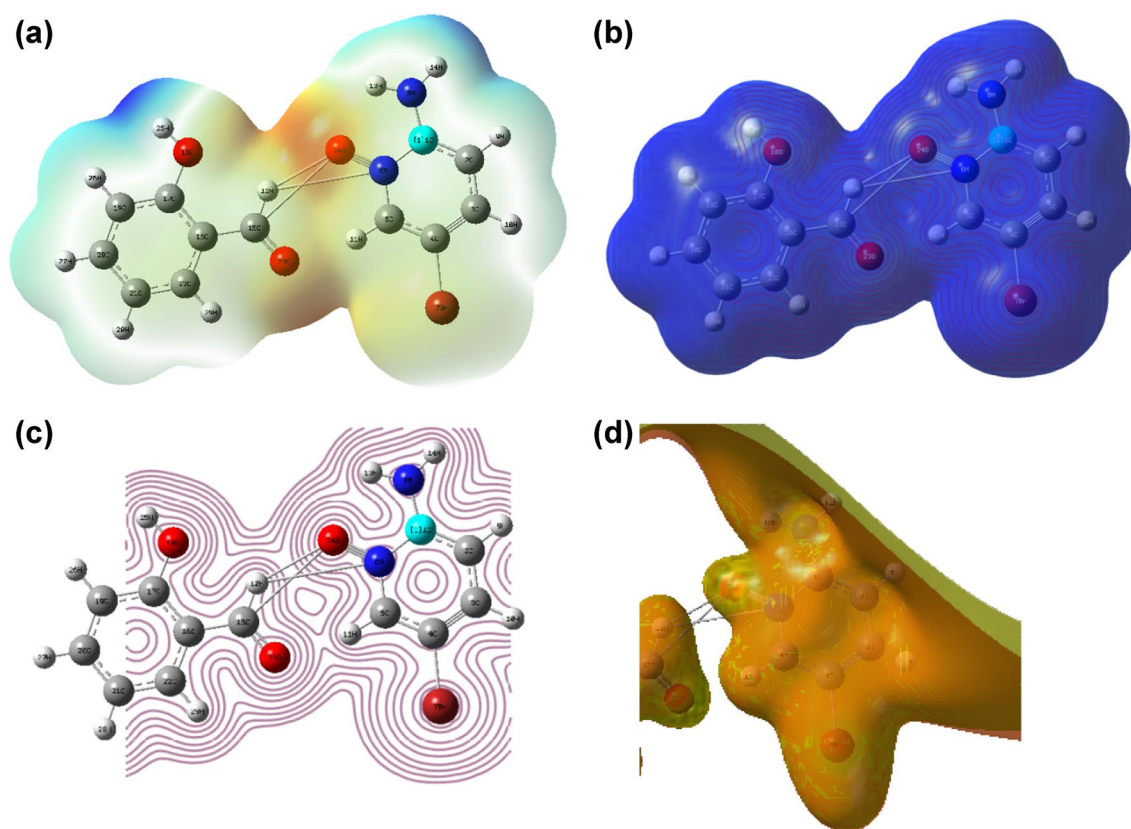


Fig. 10 **a** Molecular electrostatic potential of (MEP), **b** total electron density (TED), **c** electrostatic potential contour surface and **d** electrostatic potential of 2A5BPSA. (Color figure online)

aromatic ring. The HOMO–LUMO energy gap of 2-amino 5-bromopyridinium salicylate was calculated at the HF/6-311++G basis set method. The HOMO–LUMO energy gap of 2-amino 5-bromopyridinium salicylate $\Delta E = 5.4841$ eV. The energy gap of HOMO→LUMO explains the eventual CT interaction within the molecule, which influences the biological activity of the molecule. The HOMO–LUMO transition implies an electron density relocates to ring from amino and bromo partially from ring Table 2 represents the FMO properties of 2A5BPSA (Fig. 11).

3.11 NBO analysis

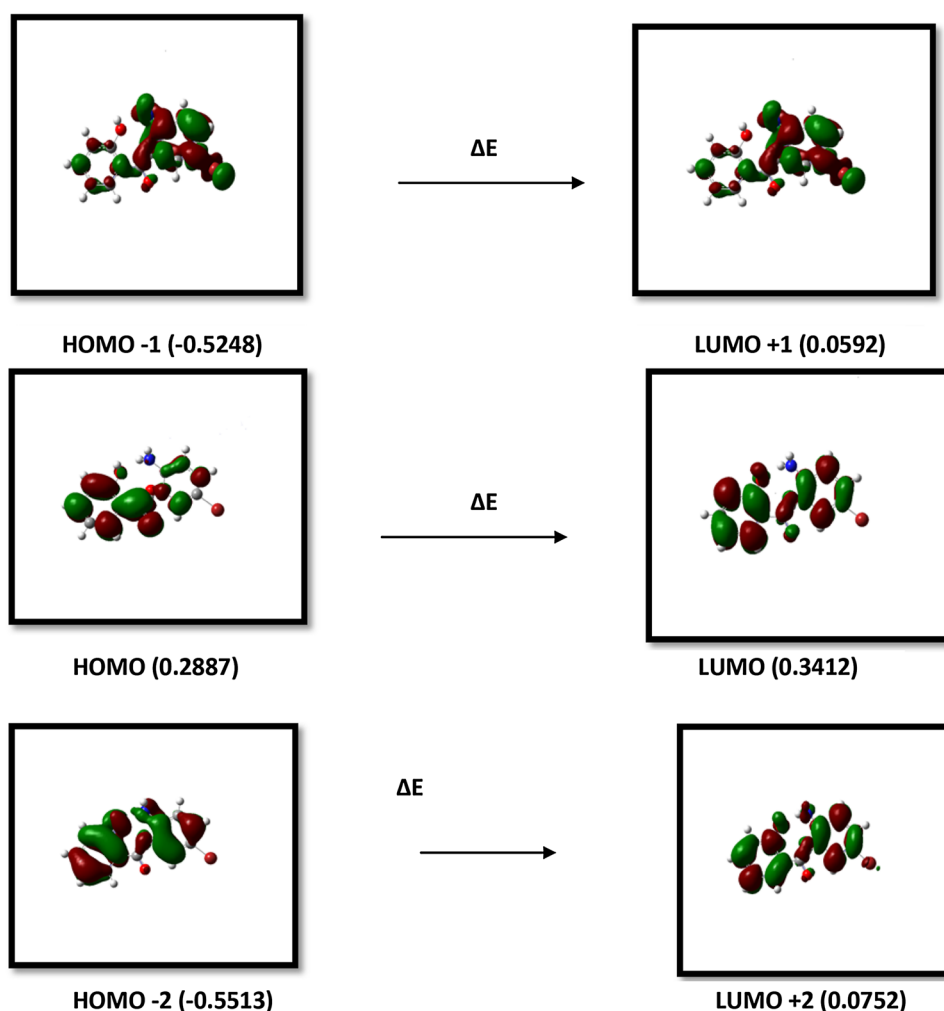
The natural bond orbital analysis provides an efficient method for studying intra- and inter-molecular bonding and interaction among bonds and also provides a convenient basis for investigating CT or conjugative interaction in molecular systems. Some electron donor orbital acceptor orbital and the interacting stabilization energy resulting from the second-order micro disturbance theory are reported. NBO analysis has been performed on the molecule at the HF/6-311++G level in order to elucidate

the intra-molecular, rehybridization and delocalization of electron density within the molecule, which are presented in Table 3. The result of interaction is a loss of occupancy from the concentration of electron NBO of the idealized Lewis structure into an empty non-Lewis orbital. For each donor (i) and acceptor (j). The stabilization energy $E(2)$ associated with the delocalization $i \rightarrow j$ is estimated as

$$E(2) = -n_{\sigma} \frac{\langle \sigma | F | \sigma^* \rangle^2}{\epsilon_{\sigma^*} - \epsilon_{\sigma}} = -n_{\sigma} \frac{F_{ij}^2}{\Delta E}$$

where $\langle \sigma | F | \sigma^* \rangle^2$ or F_{ij}^2 is the Fock matrix element i and j NBO orbitals. ϵ_{σ^*} and ϵ_{σ} are the energies of σ and σ^* NBOs, and n_{σ} is the population of the donor σ orbital. The intramolecular hyper conjugative interactions of the π – π^* transitions from (C₁–C₂, C₃–C₄) π bonds in 2A5BPSA ring lead to strong delocalization. In particular, there is a little deviation in the energetic contributions from π (C₁–C₂ and C₃–C₄) bonds to π^* (N₈–H₁₄, C₃–C₄) anti-bond transitions of 3.95 and 1.24 kcal/mol respectively. Compare

Fig. 11 Atomic orbital composition of the frontier molecular orbital for 2A5BPSA



to other contributions in the ring. The hyper conjugative interactions of the $\sigma \rightarrow \sigma^*$ transitions occur from various bonds in our molecule. Particularly σ (C_1-C_2 and C_1-N_8) having the bigger energetic contribution of their

anti-bonding σ^* (C_1-N_8 and C_1-C_2) interactions at 1.98 and 1.98e respectively.

4 Conclusions

2-amino 5-bromopyridinium salicylate (2A5BPSA) single crystal was grown from methanol solvent by slow evaporation technique. The single crystal X-ray diffraction study reveals that grown crystal belongs to the monoclinic system. The crystalline nature of grown crystal was confirmed by powder XRD studies. The functional groups present in 2-amino 5-bromopyridinium salicylate are confirmed by FTIR spectral studies. The crystal exhibits lower cut-off wavelength at 244 nm and confirms the absence of absorption in the visible region. Dielectric constant increases with respect to temperature. The photoconductivity study reveals positive photoconductivity nature of the crystal. Microhardness study confirms the soft nature of the grown crystal. Z-scan measurements reveal the locally

Table 2 Comparison of HOMO, LUMO, energy gaps and related molecular properties of 2A5BPSA crystal (eV)

Molecular properties	HF/6-31++G
E_{HOMO} (eV)	-4.9043
E_{LUMO} (eV)	0.5798
Energy gap ($E_{\text{HOMO}} - E_{\text{LUMO}}$)	5.4842
Ionization energy (IE) = $-E_{\text{HOMO}}$	4.9043
Electron affinity (EA) = $-E_{\text{LUMO}}$	-0.5798
Global hardness (η) = $1/2 (E_{\text{HOMO}} - E_{\text{LUMO}})$	-2.7420
Electronic chemical potential (μ) = $1/2 (E_{\text{HOMO}} + E_{\text{LUMO}})$	-2.1622
Global electrophilicity (ω) = $\mu^2/2\eta$	-0.8525

Table 3 second order perturbation theory analysis of Fock matrix in NBO basis for 2A5BPSA crystal

Donor (i)	Type	ED/e	Acceptor (j)	Type	ED/e	E(2) kcal/mol	E(j)–E(i) a.u.	F(i,j) a.u.
C ₁ –C ₂	σ	1.98	C ₁ –N ₈	σ*	0.01	2.06	1.52	0.05
			C ₂ –C ₃	σ*	0.02	2.36	1.73	0.057
			C ₂ –H ₉	σ*	0.007	0.9	1.59	0.034
			C ₃ –H ₁₀	σ*	0.02	2.67	1.57	0.058
C ₁ –C ₂	π	1.84	C ₃ –C ₄	π*	0.02	18.42	0.58	0.096
			C ₅ –N ₆	π*	0.76	23.3	0.3	0.089
			N ₈ –H ₁₄	σ*	0.009	3.95	0.96	0.057
C ₁ –N ₆	σ	1.94	C ₂ –H ₉	σ*	0.007	1.77	1.67	0.049
			C ₅ –N ₆	σ*	0.04	5.73	1.58	0.085
			C ₃ –H ₁₁	σ*	0.01	3.32	1.69	0.068
			N ₆ –O ₂₄	σ*	0.04	3.97	2.93	0.097
C ₁ –N ₈	σ	1.98	H ₁₂ –O ₂₄	σ*	0.06	14.21	3.63	0.203
			C ₁ –C ₂	σ*	0.02	2.2	1.76	0.056
			C ₂ –C ₃	σ*	0.02	1.57	1.78	0.047
			C ₅ –N ₆	σ*	0.04	1.66	1.55	0.046
C ₂ –C ₃	σ	1.96	N ₆ –O ₂₄	σ*	0.06	0.97	2.9	0.048
			H ₁₂ –O ₂₄	σ*	0.06	1.41	3.6	0.064
			C ₁ –C ₂	σ*	0.02	1.85	1.67	0.05
			C ₁ –N ₆	σ*	0.08	0.55	1.41	0.025
			C ₁ –N ₈	σ*	0.01	4.78	1.48	0.076
			C ₂ –H ₉	σ*	0.007	0.85	1.55	0.032
C ₃ –C ₄	σ	1.97	C ₃ –C ₄	σ*	0.02	9.45	1.97	0.122
			C ₃ –H ₁₀	σ*	0.02	1.51	1.53	0.043
			C ₄ –Br ₇	σ*	0.02	10.16	1.2	0.099
			C ₂ –C ₃	σ*	0.02	7.61	1.89	0.107
			C ₂ –H ₉	σ*	0.007	1.39	1.74	0.044
			C ₃ –H ₁₀	σ*	0.02	4.71	1.73	0.081
			C ₄ –C ₅	σ*	0.03	6.51	1.86	0.098
C ₃ –C ₄	π	1.81	C ₄ –Br ₇	σ*	0.02	0.71	1.39	0.028
			C ₅ –H ₁₁	σ*	0.01	1.45	1.77	0.045
			C ₁ –C ₂	π*	0.22	34.23	0.54	0.123
			C ₃ –C ₄	π*	0.288	1.24	0.61	0.025
C ₄ –C ₅	σ	1.97	C ₅ –N ₆	π*	0.76	26.56	0.32	0.098
			C ₃ –C ₄	σ*	0.02	8.25	2.02	0.115
			C ₃ –H ₁₀	σ*	0.02	6.17	1.58	0.088
			C ₅ –N ₆	σ*	0.04	1	1.51	0.035
			C ₃ –H ₁₁	σ*	0.01	1.8	1.62	0.048
C ₄ –Br ₇	σ	1.97	N ₆ –O ₂₄	σ*	0.04	5.51	2.85	0.112
			C ₂ –C ₃	σ*	0.02	6.73	1.62	0.093
			C ₃ –C ₄	σ*	0.02	1.79	1.9	0.052
			C ₃ –H ₁₀	σ*	0.02	1.52	1.46	0.042
			C ₄ –C ₅	σ*	0.03	0.65	1.59	0.029
C ₅ –N ₆	σ	1.95	C ₅ –N ₆	σ*	0.04	7.47	1.39	0.091
			C ₁ –C ₂	σ*	0.02	0.69	1.9	0.033
			C ₁ –N ₆	σ*	0.08	12.52	1.64	0.129
			C ₁ –N ₈	σ*	0.01	1.7	1.71	0.049
			C ₄ –C ₅	σ*	0.03	1.23	1.89	0.043
			C ₄ –Br ₇	σ*	0.02	2.02	1.42	0.048
C ₅ –N ₆	π	1.79	N ₆ –O ₂₄	σ*	0.04	52.43	3.03	0.356
			H ₁₂ –O ₂₄	σ*	0.06	1.73	3.73	0.072
			C ₁ –C ₂	π*	0.22	15.56	0.64	0.09

Table 3 (continued)

Donor (i)	Type	ED/e	Acceptor (j)	Type	ED/e	E(2) kcal/mol	E(j)–E(i) a.u.	F(i,j) a.u.
C ₅ –H ₁₁	σ	1.98	C ₃ –C ₄	π*	0.288	25.65	0.71	0.123
			C ₅ –N ₆	π*	0.76	34.08	0.42	0.126
			C ₁ –N ₆	σ*	0.08	3.41	1.2	0.058
			C ₃ –C ₄	σ*	0.02	4.59	1.77	0.081
			C ₄ –C ₅	σ*	0.03	2.42	1.46	0.053
N ₆ –O ₂₄	σ	1.96	C ₅ –N ₆	σ*	0.04	0.86	1.25	0.029
			C ₁ –C ₂	σ*	0.02	3.46	3.17	0.094
			C ₁ –N ₆	σ*	0.08	10.57	2.9	0.158
			C ₅ –N ₆	σ*	0.04	7.88	2.95	0.137
			N ₆ –O ₂₄	σ*	0.04	0.82	4.3	0.053
N ₈ –H ₁₄	σ	1.98	H ₁₂ –O ₂₄	σ*	0.06	75.42	5	0.552
			C ₁ –C ₂	π*	0.22	2.23	0.98	0.044
			C ₁ –N ₆	σ*	0.08	4.93	1.34	0.074
H ₁₂ –O ₂₄	σ	1.85	C ₁ –N ₆	σ*	0.08	25.72	2.44	0.227
			C ₅ –H ₁₁	σ*	0.01	0.7	2.6	0.039
			N ₆ –O ₂₄	σ*	0.04	16.83	3.83	0.233
C ₁ –C ₂	π	1.84	C ₃ –C ₄	π*	0.288	66.81	0.07	0.117
C ₅ –N ₆	π	1.79	C ₁ –C ₂	π*	0.22	15.75	0.22	0.074
			C ₃ –C ₄	π*	0.288	37.14	0.28	0.126

induced thermo-optic effect. The DFT explained the HOMO–LUMO and natural bonding analysis properties of 2-amino 5-bromopyridinium salicylate explained in detail. All above results suggesting that the grown 2A5BPSA can act as a potential candidate for optoelectronics applications.

References

- P. Vivek, A. Suvitha, P. Murugakoothan, *Spectrochim. Acta A* **134**, 517–525 (2015)
- M. Krishna Kumar, S. Sudhakar, P. Pandi, G. Bhagavannarayana, R. Mohan Kumar, *Opt. Mater.* **36**, 988–995 (2014)
- B. Dhanalakshmi, S. Ponnusamy, C. Muthamizhchelvan, V. Subhashini, *Mater. Res. Bull.* **70**, 809–816 (2015)
- A.S. Amin, G.O. El-Sayed, Y.M. Issa, *Analyst* **120**, 1189–1193 (1995)
- F.L. Zhao, B.Z. Xu, Z.Q. Zhang, S.Y. Tong, *J. Pharm. Biomed. Anal.* **21**, 355–360 (1999)
- D.S. Chemla, J. Zyss, *Nonlinear Optical Properties of Organic Molecules and Crystals* (Academic Press, Orlando, 1987) pp. 1–2
- L. Jothi, K. Ramamurthi, *Indian J. Sci. Technol.* **4**, 6 (2011)
- V. Murugesan, M. Saravanabhavan, M. Sekar, *J. Mol. Struct.* **1084**, 95–102 (2015)
- K. Thirupugalmani, S. Karthick, G. Shanmugam, V. Kannan, B. Sridhar, K. Nehru, S. Brahadeeswaran *Opt. Mater.* **49**, 158–170 (2015)
- N. Ramamurthy, S. Dhanuskodi, M.V. Manjusha, J. Philip, *Opt. Mater.* **33**, 607–612 (2011)
- M. Rajalakshmi, R. Indirajith, M. Palanichamy, R. Gopalakrishnan, *Spectrochim. Acta A* **84**, 43–50 (2011)
- L. Chandra, J. Chandrasekaran, K. Perumal, B. Babu, *Optik* **127**, 3206–3210 (2016)
- V. Meenatchi, K. Muthu, M. Rajasekar, S.P. Meenakshisundaram, S.C. Mojumdar, *J. Therm. Anal. Calorim.* **108**, 895–900 (2012)
- M. Amudha, R. Rajkumar, V. Thayanthi, P. Praveen Kumar, *Adv Opt. Technol.* (2015). doi:10.1155/2015/206325
- C.K. Quah, M. Hemamalini, H.-K. Fun, *Acta Cryst. Sec. E* **E66**, o2164–o2165 (2010)
- K. Sathishkumar, J. Chandrasekaran, B. Babu, C.I. Sathish, Y. Matsushita, *Appl. Phys. A* **119**, 1355–1364 (2015)
- B. Mohanbabu, R. Bharathikannan, G. Siva, *J. Optoelectron. Adv. Mater.* **17**, 1603–1614 (2015)
- A. Silambarasan, M. Krishna Kumar, A. Thirunavukkarasu, R. Mohan Kumar, P.R. Umarani, *Spectrochim. Acta Part A* **135**, 39–45 (2015)
- M. Mohammadikish, F. Davar, M.R. Loghman-Estarki, Z. Hamidi, *Ceram. Int.* **39**, 3173 (2013)
- M. Mohammadikish, F. Davar, M.R. Loghman-Estarki, Z. Hamidi, *Cryst. Eng. Commun.* **14**, 7338 (2012)
- B. Babu, J. Chandrasekaran, B. Mohanbabu, Yoshitaka Matsushita, M. Saravanakumar. *RSC Adv.* **6**, 110884 (2016)
- S. Balaprabakaran, J. Chandrasekaran, B. Babu, R. Thirumurugan, K. Anitha, *Spectrochim. Acta A* **136**, 700–706 (2015)
- R. Thirumurugan, B. Babu, K. Anitha, J. Chandrasekaran, *Spectrochim. Acta Part A* **140**, 44–53 (2015)
- V.N. Joshi, *Photoconductivity*, (Marcel Dekker, New York, 1990)
- B.W. Mott, *Micro-Indentation Hardness Testing* (Butterworths, London, 1956), p. 206
- E. Mayer, *Z. Ver. Dtsch. Ing.* **52**, 645 (1908)
- E.M. Onitsch, *Microscopia* **2**, 131–151 (1947)
- M. Hanneman, *Metall. Manch* **23**, 135–140 (1941)
- B. Babu, J. Chandrasekaran, S. Balaprabakaran, *Mater. Sci.–Pol.* **32**, 164–170 (2014)
- M. Sheik-Bahae, A. A. Said, Van E. W. Stryland, *Opt. Lett.* **14**, 955 (1989)

31. M. Sheik-Bahae, A.A. Said, T.H. Wei, D.J. Hagan, E.W. Van Stryland, *IEEE J. Quantum. Electron.* **26**, 760–769 (1990)
32. R.W. Boyd, *Nonlinear Optics*, 2nd ed. (Academic Press, New York, 2003)
33. A. Hakan, A. Öztekin, *Int. J. Mol. Sci* **8**, 760–776 (2007)
34. N. Sundaraganesan, S. Illakiamani, H. Saleem, P.M. Wojciechowski, D. Michalska, *Spectrochim. Acta A* **61**, 2995–3001 (2005)
35. Gaussian 09 Program, *Revision C.01*, J. Frisch, et al. (Gaussian, Inc., Wallingford CT, 2010)
36. A.D. Becke, *J. Chem. Phys.* **98**, 5648–5652 (1993)
37. G. Rauhut, P. Pulay, *J. Phys. Chem* **99**, 3093–3100 (1995)
38. R.I. Dennington, T. Keith, J. Millam, K. Eppinnett, W. Hovell, *Gauss View Vers. 3 9*, (2003)